

The Stellar Content of the Halo of NGC 5907 from Deep HST NICMOS Imaging¹

Stephen E. Zepf

Department of Astronomy, Yale University, New Haven, CT 06520;
 zepf@astro.yale.edu

Michael C. Liu

Department of Astronomy, University of California, Berkeley, CA 94720;
 mliu@astro.berkeley.edu

Francine R. Marleau

Institute of Astronomy, University of Cambridge, Cambridge CB3 0HA, U.K.;
 marleau@ast.cam.ac.uk

Penny D. Sackett

Kapteyn Institute, University of Groningen, 9700 AV Groningen, Netherlands;
 psackett@astro.rug.nl

James R. Graham

Department of Astronomy, University of California, Berkeley, CA 94720;
 jrg@astro.berkeley.edu

ABSTRACT

We present H-band images obtained with NICMOS of a field $75''$ (5 kpc) above the plane of the disk of the edge-on spiral galaxy NGC 5907. Ground-based observations have shown that NGC 5907 has a luminous halo with a shallow radial profile between 4 and 8 kpc that roughly traces the dark matter distribution of the galaxy deduced from its rotation curve. Our NICMOS observations were designed to resolve bright giants in the halo of NGC 5907 to constrain its stellar composition with the goal of understanding its nature and origin. More than 100 stars are expected in the NICMOS images if the dwarf-to-giant ratio in the halo of NGC 5907 is consistent with that expected from standard stellar initial mass functions, and if ground-based estimates of the distance to NGC 5907 and the integrated colors of its halo are correct. Instead we observe only one candidate giant star. This apparent discrepancy can be resolved by assuming either a significantly larger distance than suggested by several studies,

¹Based on observations with the NASA/ESA Hubble Space Telescope, obtained at the Space Telescope Science Institute, which is operated by the Association of Universities for Research in Astronomy, Inc., under NASA contract NAS 5-26555.

or a halo metallicity much lower than suggested by ground-based colors and as low as metal-poor Galactic globular clusters. If previous distance and halo color estimates for NGC 5907 are correct, our NICMOS results suggest that its extended light is composed of stars that formed with an initial mass function different than that observed locally, leading to a much higher ratio of dwarfs to giants. We describe how these three possible explanations for the absence of bright giants in our NICMOS images of the halo of NGC 5907 might be constrained by future observations.

Subject headings: galaxies: halos — galaxies: individual (NGC 5907) — galaxies: stellar content — infrared: galaxies

1. Introduction

The presence of dark matter halos around galaxies is well-established through a number of observations. These include the flat rotation curves of spiral galaxies, the velocities of globular clusters and satellites around their host galaxies, the properties of hot X-ray gas around ellipticals, and mass-to-light ratio measurements from gravitational lensing (e.g. reviews by Sackett 1996, Ashman 1992, Trimble 1987). However, despite this wealth of data demonstrating the existence of massive dark halos, their composition remains unknown.

The total mass density inferred for galaxy halos is roughly $\Omega_{galaxies} \simeq 0.2$ (e.g. Bahcall, Lubin, & Dorman 1995). This number comes from the combination of the observed luminosity density in the local universe (e.g. Loveday et al. 1992, Efstathiou et al. 1988) with the assumption that typical galaxy halos extend to ~ 200 kpc, as suggested by observations of satellites of spiral galaxies (Zaritsky et al. 1993), and have $(M/L)_B \simeq 100h$ within this radius around spirals and a factor of a few higher around ellipticals (e.g. Mushotzky et al. 1994). The best constraint on the corresponding value of the mass density in baryons comes from measurements of deuterium in quasar absorption lines, from which $\Omega_B h^2 \simeq 0.02$ is derived (Burles & Tytler 1998a,b). For current estimates of $H_0 = 70 \text{ kms}^{-1}\text{Mpc}^{-1}$ (Mould et al. 1999), this baryonic density is smaller than the total mass density inferred for galaxy halos, indicating that some or most of the dark matter around galaxies is in the form of exotic particles. Nevertheless, Ω_B is not negligible compared to $\Omega_{galaxies}$, leaving room for a substantial contribution from baryons to the massive dark halos around galaxies.

Photometry of edge-on spiral galaxies in search of massive halos has been done since the 1970s, originally with TV cameras and photographic plates (e.g. Davis 1975). Faint, extended halo light is easiest to detect in thin, edge-on spirals because the regions above and below the galactic plane are not contaminated through projection effects by the brighter stellar disk. Skrutskie et al. (1985) set upper limits on faint V -band and, using large apertures, K -band emission in the late type edge-on spirals NGC 2683, NGC 4244 and NGC 5907, concluding that no more than

$\simeq 1/3$ of an isothermal dark halo could be composed of a luminous baryonic component. Refined halo mass models for NGC 5907 based on galaxy parameters derived in H and K from pixelated near-infrared detectors and the Skrutskie et al. (1985) upper limits for halo light increased the baryonic upper limit to $\simeq 2/3$ (Barnaby & Thronson 1994).

NGC 5907 is a particularly interesting case since it exhibits a flat rotation curve well beyond its Holmberg radius (Sancisi & van Albada 1987, Sofue 1994) which allows a good estimate of its dynamical mass to be made. The thin stellar disk is slightly warped perpendicular to the line-of-sight. In a pioneering CCD photometry study of very low surface brightness features around edge-on spiral galaxies by Morrison, Borošon, & Harding (1994), faint extended R -band emission was discovered around NGC 5907. The extended light is unlike any known thick disk, both in terms of its shallow radial profile and its low surface brightness (Sackett et al. 1994, Morrison 1999). However, the faint NGC 5907 light is well fit with a halo-like profile that is moderately flattened toward the plane of the galaxy ($c/a \approx 0.5$) and a radial volume density profile $\rho \propto r^{-2.3}$, similar to that inferred for the massive halo from the rotation curve (Sackett et al. 1994). A similar flattening has also been tentatively observed in the globular cluster system of NGC 5907 in a recent study with HST by Kissler-Patig et al. (1999).

The R -band radial profile of the NGC 5907 halo is considerably shallower than that of known stellar populations in the halos of the Milky Way and M31, which are much steeper than that of the dark halo mass inferred from their rotation curves and other dynamical measures. Specifically, in the Galaxy the RR Lyrae distribution falls off as roughly $r^{-3.5}$ (Saha 1985) and the globular cluster system as r^{-3} (Zinn 1985) or $r^{-3.5}$ (Harris & Racine 1979). In M31, the globular clusters are distributed like r^{-3} (Racine 1991), while red giant branch stars appear to have a profile falling at least as steeply as $r^{-3.8}$ (Reitzel, Guhathakurta, & Gould 1998). In contrast, various kinematical and lensing constraints suggest that the total mass distribution of our Galaxy and other spirals has a much shallower radial profile, perhaps r^{-1} within a few kpc and tapering to roughly r^{-2} out to at least 50 kpc and perhaps much beyond (Sackett 1996, 1999 and references therein; Zaritsky 1999 and references therein).

The existence of this unusual stellar component with a shallow radial profile in NGC 5907 has been confirmed by a number of independent observations by other groups, both in the near-infrared (Rudy et al. 1997, James & Casali 1998) and at other optical wavelengths (Lequeux et al. 1996, 1998, Zheng et al. 1999). Although different proposals have been made for the origin of the extended light in these studies, all radial profiles agree at surface brightness levels of $R \leq 27$ mag/arcsec 2 , corresponding to a height above the plane of about 120'' (8 kpc for a distance of 14 Mpc). Lequeux et al. report optical colors for this shallow, extended population of $(B - V) \simeq 1.0$ and $(V - I) \simeq 1.4$, as red as typical elliptical galaxies, while red $J - K$ colors of 1 – 1.5 have been reported in the infrared studies (Rudy et al. 1997, James & Casali 1998). At longer wavelengths of 3.5 - 5 μ m, Yost et al. (1999) have recently reported a non-detection around NGC 5907 at 180'' to 540'' (12 – 37 kpc). Combining this result with model atmospheres, they conclude that hydrogen burning stars contribute no more than 15% of the dark mass within this

region. Although this non-detection at $3.5 - 5\mu\text{m}$ does not coincide spatially with the detections at $\leq 2.2\mu\text{m}$, the negative result at longer wavelengths suggests that whatever produces the faint optical light around NGC 5907 does not emit strongly at these wavelengths and probably does not have enough mass to account for the dark matter halo inferred from the rotation curve.

The origin of the stellar halo of NGC 5907 raises many puzzles. Its shallow radial profile differs from known disk populations and red colors are different from known halo populations. The relatively red color implies either an initial mass function (IMF) favoring extremely low mass dwarfs ($< 0.2M_\odot$), or a normal, metal-rich, old stellar population. Stellar halos are expected to be metal-poor, as observed in the Milky Way, because halo formation is believed to occur early in the life of a galaxy before the majority of metals have been generated in nuclear processes in stellar interiors. But an IMF as strongly biased towards low mass dwarfs as is required to explain the halo colors of NGC 5907 has not been observed in globular clusters or in the local halo population of the Milky Way (e.g. King et al. 1998 and references therein). On the other hand, if the red colors are generated by an old, metal-rich population, one must explain how such a population came to reside in the halo where metal enrichment is thought to be low.

One possibility proposed by Lequeux et al. (1998) is that such a halo could result from accretion of a metal-rich population from a low-mass elliptical after a tidal encounter with NGC 5907. If such an encounter could disrupt the elliptical without damaging the thin disk of NGC 5907, the debris may naturally settle into a halo configuration similar to what is observed. Alternatively, Fuchs (1995) suggests the extended halo population originates from the dynamical response of the stellar spheroid to the dark matter halo in which it is embedded. Zheng and collaborators suggest that the faint light seen in their deep observations of NGC 5907 — and by inference the observations of others as well — may be a combination of effects including confusion from a very narrow arc apparently associated with the galaxy, an unseen but postulated face-on warp, and stellar foreground confusion. If these suggestions, all of which involve normal stellar populations, are correct, the surface brightness observed from the ground should be associated with a substantial number of giants that can be resolved from space.

In this paper, we present and discuss the implications of NICMOS observations of the halo of NGC 5907 designed to detect the many individual bright giants expected to contribute significantly to the halo light of NGC 5907 if it is composed of a stellar population with a initial mass function like that observed locally and has a distance and colors consistent with existing observations. In Section 2, we describe the observations, data reduction and analysis including the detection limits, and show the resulting mosaic of our images of the stellar halo of NGC 5907. The comparison of these observations to models of the stellar population of this component is presented in Section 3. This section includes a detailed discussion of the effects of distance, metallicity, and initial mass functions on these models and thus the interpretation of our data. The implications of the absence of stellar sources in our H-band images of the observed stellar halo of NGC 5907 are discussed in Section 4.

2. Observations and Data Reduction

We used the near-infrared camera (NICMOS; MacKenty et al. 1997) on the Hubble Space Telescope (HST) to observe a field in the halo of NGC 5907 during two separate observing windows on 1998 May 23 and 1998 July 10-11. A total 35,326 s of integration time over 12 orbits was obtained. One dark exposure of zero length was taken at the beginning of each orbit in the ACCUM mode to reduce persistence effects from cosmic rays, and the remainder were taken through the F160W filter in the MULTIACCUM mode with the SPARS64 sequence. Between the two separate observing windows, the position angle of the telescope was free to rotate and rolled clockwise by 43.7 deg. Observations were obtained with the NIC2 camera, which has a field of view $19.^{\circ}2 \times 19.^{\circ}2$ wide with 256 pixels on a side and $0.^{\circ}075$ per pixel. The telescope was pointed so that the geometrical center of the NIC2 camera was $\alpha = 15^{\text{h}}16^{\text{m}}01^{\text{s}}.54$, $\delta = 56^{\text{deg}} 20'31.^{\prime\prime}7$ (J2000). This location is $75.^{\prime\prime}$ away from the center of the galaxy, perpendicular to the plane of the galaxy (Figure 1), corresponding to a distance above the plane of the galaxy of 5.1 kpc based on a distance to NGC 5907 of 14 Mpc (see Section 3.3 for a discussion of the distance to the galaxy). This position was chosen to be outside both the region of disk confusion and the thin, long arc found by Shang et al. (1998), but well inside the region where extended light has been reported in BVRIJK.

The images were processed through CALNICA, the standard NICMOS pipeline, which performs bias subtraction, dark-count correction, and flat-fielding. Our own subsequent data reduction consisted of masking bad pixels, correcting for constant offsets between the four quadrants of the NIC2 camera, and subtracting a scaled master “sky frame” constructed from the average of all of the individual images. The images were then registered and combined. Due to the different position angles between visit 1 and visit 2+3, the images of visit 1 were combined separately from visit 2+3. The images of visit 2+3 were registered with respect to each other using the brightest object in the field and co-added to improve the signal-to-noise. The first image of visit 3 was not included in the combined image because of bad trailing due to the loss of one of our guide stars during that exposure. The visit 1 mosaic, generated using the world coordinate system in the image, was then combined with visit 2+3, after rotating the latter by an angle of 43.7 deg and registering on the brightest object in the field. The rotation was done after mosaicing because rotation spreads bad pixels and cosmic ray hits in a way that it is difficult to remove them accurately when combining individually rotated images. Each resulting mosaic covers a field of view $23.^{\circ}75 \times 20.^{\circ}25$ wide. The final combined F160W image of our field is shown in Figure 2. The signal-to-noise ratio is higher at the center of the image, where the total integration time is longer, and lower at the edges of the frames.

2.1. Photometry

Photometry was performed on the final combined image using the version of the automated star-detection algorithm DAOPHOT (Stetson 1992) as implemented in the IRAF package. In order to allow a uniform threshold for object detection to be applied across the whole image, each pixel in the image was normalized by the square-root of the exposure time at that location. The object detection was performed with the subroutine DAOFIND and a detection threshold of 5σ above the local background level. Objects were also required to have DAOPHOT parameters $-0.5 < \text{SHARP} < 0.5$ and $\text{CHI2} < 5$. These cuts are aimed at eliminating features that have a significantly smaller or larger extent than the PSF (e.g. cosmic rays or single pixel defects and unresolved blends or large galaxies, respectively). Only one object meets these criteria and is a potential star. This object is also the only object with a FWHM less than twice the FWHM of the PSF.

The single stellar object detected is marked on Figure 2 with a circle. The total magnitude of that star is $m_{\text{F160W}} = 23.6$. This is determined by obtaining photometry in an aperture of 1.7 pixels in diameter and using an aperture correction derived either from TINYTIM models or NIC2 observations of brighter stars in other fields (these give the same results). The magnitudes in the F160W filter are very similar to typical ground-based H-band magnitudes, with an uncertainty in the calibration of NICMOS photometry for an object with unknown color of about 10% (Colina & Rieke 1997). Due to the high Galactic latitude of NGC 5907 ($b = 51$ deg), models of the stellar distribution in the Galaxy yield a negligible probability of a foreground star in our field (e.g. Cohen et al. 1993). However, there are few constraints on Galactic sub-stellar (e.g. brown dwarf) populations at these very faint infrared magnitudes. Based on deep NICMOS pointings in blank areas of the sky (e.g. Yan et al. 1998), we expect roughly ten faint field galaxies in the images, consistent with the number of resolved sources we detect.

2.2. Artificial Star Tests

In order to determine the magnitude limit of our photometry, we performed a series of artificial star tests on the images. Specifically, we added artificial stars of known magnitude into the final NIC2 image used for the analysis above, and then performed the same object detection and photometry on these images with the artificial stars that was used on the original image. Because of the lack of stellar objects in our field, we used a PSF determined from other NIC2 data (Marleau et al. 1999) to create the artificial stars. For each 0.1 magnitude bin, 105 artificial stars were added to the original image with a random spatial distribution. The object identification and output magnitudes for the artificial stars that were returned by the same procedures used on the real data were then compared to the input list. This was repeated three times for each 0.1 magnitude bin, and the results averaged for each bin. A plot of the recovery fraction (completeness) as a function of input magnitude is given in Figure 3. As shown in this

plot, the average completeness of the photometry over the full image is 50% for objects with $m_{F160W} = 24.9$.

3. Results

3.1. Fiducial Model

The primary goal of our work is to constrain the nature of the halo of NGC 5907 by comparing the observed star counts in our NICMOS image to the star counts expected for various models of the stellar population of the halo of NGC 5907. Our procedure is to take a luminosity function in F160W for a given stellar population, either from observations such as those in the Galactic bulge, or from theoretical models, place this population at the distance of NGC 5907, and normalize the luminosity function to match the observed surface brightness within the region of our NICMOS data. We then convert this into a prediction of the number of stars expected in our NICMOS images by multiplying the predicted distribution in apparent magnitudes with the completeness function determined above.

We begin by considering a fiducial model, based as closely as possible on the observed properties of NGC 5907 and its extended light distribution. Specifically, our fiducial model has a surface brightness within the NICMOS region of $R = 25.85$ mag/arcsec 2 as measured by Morrison et al. (1994), a distance to NGC 5907 of 14 Mpc based both on Tully-Fisher and models for deviations from the Hubble flow in the region around NGC 5907 (see Section 3.3), and an H-band stellar luminosity function adapted from studies of Baade’s window (Tiede et al. 1995), which has a metallicity similar to that suggested by the observed broad-band colors of the extended stellar light in NGC 5907. This fiducial model predicts that more than 100 stars should be seen in the combined NICMOS image, in stark contrast to our observation of one candidate star. This is graphically demonstrated in Figure 4, in which we simulate the expected appearance of the fiducial model in our NICMOS image, accounting for the expected Poisson shot noise. The significant number of bright giants expected for the simplest assumptions about the stellar population in the halo of NGC 5907 are not present in the data. Because of the stark difference between the observations and the simplest prediction, we consider in turn each of the components that go into the prediction. A fundamental component of our calculation is the H-band luminosity function, which depends on the initial mass function (IMF), metallicity, and age of the stellar population. The distance to NGC 5907 and the surface brightness of its halo within our NICMOS field also play a role and we consider all of these below.

3.2. Luminosity Function, IMF, and Metallicity

For the fiducial case shown in Figure 4, we adopt an H-band stellar luminosity function constructed from the K-band luminosity function observed in Baade’s Window (Tiede et al. 1995), adjusted to F160W by a small color term. The choice of a luminosity function based on the Galactic Bulge is motivated by the similar metallicities of stars in Baade’s Window (e.g. McWilliam & Rich 1994) and the halo of NGC 5907, as inferred from its optical colors as described in detail below. This approach also has the benefit of comparing the data to an empirical luminosity function. As demonstrated in Figure 4, the luminosity function based on observations in Baade’s Window dramatically fails to account for the data.

Because of the failure of the fiducial model, we explored a range of stellar initial mass functions and metallicities to search for sets of parameters that are consistent with the data. We generated theoretical F160W luminosity functions using the single burst 12 Gyr-old stellar population synthesis models of Bruzual & Charlot (1998) with the semi-empirical stellar spectral energy distributions of Lejeune, Cuisinier, & Buser (1997). The models are defined for $[\text{Fe}/\text{H}] = -2.3, -1.7, -0.7, -0.4, 0.0, +0.4$ with a stellar mass range of $0.1 - 125 M_{\odot}$. We also consider a range of stellar initial mass functions, parametrized as a single power law with slope α , such that $dN = M^{-(\alpha+1)}dM$, where a Salpeter IMF is $\alpha = 1.35$. We caution that the stellar population models become unreliable for $\alpha \gtrsim 4$ because at these very steep slopes the stars at the bottom of the main sequence become the principal contributors to the integrated light. In this case, the accuracy of the model predictions rests on the assumed colors of old late-type M dwarfs and the shape of the IMF near the hydrogen burning limit, both of which are poorly constrained locally, much less as a function of metallicity. Nevertheless, the qualitative behavior of the models for cases of extremely large α should be correct, even if they are more uncertain quantitatively.

Figure 5 shows H-band luminosity functions predicted for our NICMOS observations of the halo of NGC 5907 as a function of IMF slope and metallicity, given the ground-based observations of the R-band surface brightness of 25.85 magnitudes/arcsec² (§3.4), a distance to NGC 5907 of 14 Mpc (§3.3), and the completeness function shown in Figure 3 (§2.2). Figure 5 shows that only extremely steep IMFs or very low metallicities are consistent with our NICMOS data in which only one possible star is detected. In the former case, the absence of giants originates in an extraordinarily higher dwarf to giant ratio in the stellar halo of NGC 5907, while in the latter, low-metallicity giants are simply too faint to be detected because of the dependence on metallicity of the brightness of giants in the H-band.

This result can be quantified further by considering the Poisson statistics of either one or zero detected stars. For metallicities of $[\text{Fe}/\text{H}] \geq -0.7$, even the largest α we consider is discrepant with the observation of one star at $> 99.99\%$ confidence level. Because of the uncertainties in the stellar populations models in these extraordinarily dwarf dominated IMFs discussed above, we simply adopt $\alpha > 4$ as the result for $[\text{Fe}/\text{H}] \geq -0.7$. Alternatively, if $[\text{Fe}/\text{H}]$ is sufficiently low, then the brightest giants become too faint to detect. If one adopts the usual Salpeter IMF

with $\alpha = 1.35$, this requires $[\text{Fe}/\text{H}] \lesssim -1.7$. As can be seen in Figure 5, the transition from the presence of giants at $[\text{Fe}/\text{H}] \geq -0.7$ to the absence of giants at $[\text{Fe}/\text{H}] \lesssim -1.7$ is fairly insensitive to modest changes in α . We also note that if the light in NGC 5907 is assumed to come from a solely low metallicity population, the one stellar object is unlikely to be a star in the halo of NGC 5907, since the low metallicity models predict that any stars that are detected are found at the faintest limit of the data, while the stellar object is more than one magnitude brighter than our 50% completeness limit.

Tighter constraints on the stellar population of the extended light around NGC 5907 can be placed by requiring the integrated colors of the halo population to be consistent with the ground-based colors of the halo light reported by Lequeux et al. (1998). Figure 6 compares the observed (B–V) and (V–I) colors to the BC98 model populations over the same range of α and $[\text{Fe}/\text{H}]$ shown in Figure 5. With the NICMOS data alone, it is possible to account for the absence of giants through very low metallicity since then the giants would be too faint to detect in our images. Figure 6 shows that the published optical colors argue against the possibility of a very low metallicity with a normal IMF. We also note that the near-infrared (J–K) colors of Rudy et al. (1997) and James & Casali (1999) are even redder than the models that can account the optical colors, which are already red. While it is unclear whether the problem is with these challenging observations, or with difficulties in the models for either the reddest metal-rich giants (important for populations with normal IMFs) or the latest type M dwarfs (important for the steep IMFs), it is clear that the observational evidence to date suggests that the colors of the NGC 5907 halo are red. Therefore, the joint NICMOS star count and color constraints appear to require a dramatically higher dwarf-to-giant ratio than given by a typical IMF.

More quantitatively, in order to be consistent within the 99% confidence limit of our observation of only a single star in the NICMOS field, the ratio of bright giants to fainter stars must be more 100 times lower than that expected for a stellar population with a Salpeter IMF and a metallicity that is consistent with the optical colors at the 2σ level. This constraint translates to $\alpha > 3$ for a simple power-law parametrization of the IMF. Such steep IMFs cause low metallicity models which are consistent with the absence of bright giants ($[\text{Fe}/\text{H}] \lesssim -1.7$) to become red enough to begin to match the optical colors. Because this result indicates a much higher ratio of dwarfs to giants than observed in Galactic globular clusters or expected from the stellar initial mass function in star forming regions of the Galaxy, we examine the robustness of each of the steps taken in obtaining this result.

3.3. Distance

The detection of bright giants in NGC 5907 clearly depends on the distance to the galaxy. Using both the H and R-band Tully-Fisher relations, as well as the observed radial velocity of NGC 5907 combined with a model of the expected peculiar velocity at its location, we find that NGC 5907 is at a distance of 14 Mpc, with an uncertainty of 20%. Half of this uncertainty is

due to the intrinsic scatter of the techniques we use to determine the distance to NGC 5907. The other half is due to the current uncertainty in the extragalactic distance scale, as manifested in the uncertainty in the distance to the Virgo cluster or similarly in the Hubble constant. This comes primarily from the uncertainty in the absolute calibration of the Cepheid Period-Luminosity relation. A distance to NGC 5907 of 14 Mpc is somewhat greater than that typically adopted in earlier work (e.g. Morrison et al. 1994), and our own preliminary presentation of this work at conferences (Liu et al. 1998).

3.3.1. *H*-band Tully-Fisher

The H-band Tully-Fisher relation is one of the most reliable methods for determining distances to edge-on spiral galaxies like NGC 5907. The Tully-Fisher relation has been heavily studied and tested, resulting in well-established relationships between spiral galaxy luminosity and line-width (e.g. Jacoby et al. 1992). Moreover, the H-band offers a significant advantage in its reduced sensitivity to internal extinction, which is the dominant source of uncertainty for optical determinations of the magnitudes of edge-on galaxies. Even in H, the internal extinction is probably not zero for galaxies as inclined as NGC 5907 (e.g. Moriondo, Giovanelli, & Haynes 1998, Tully et al. 1998).

One way to determine the H-band Tully-Fisher distance to NGC 5907 is to adopt the H-band Tully-Fisher relation given by Hubble Space Telescope Key Project on the Hubble Constant, which is based on Cepheid distances to 21 spiral galaxies (Sakai et al. 1999). Specifically, the Key Project team found an H-band Tully-Fisher relation of $H_{-0.5}^c = -11.03(\log W_{20}^c - 2.5) - 21.74$, where $H_{-0.5}^c$ is the H-band magnitude within an aperture that is a fixed fraction of the B-band diameter, as defined by Aaronson, Huchra, & Mould (1979), and W_{20}^c is the velocity width of HI at 20% of the maximum HI flux, corrected for inclination. The observed dispersion in the relation is 0.36 magnitudes for the Key Project sample, similar to that found for samples of cluster spirals (e.g. Peletier & Willner 1991, 1993; hereafter PW91 and PW93). The slope of this H-band Tully-Fisher relation is similar to, but slightly larger than that found for spirals in Virgo and Ursa Major found by PW91 and PW93, and by the earlier work of Aaronson, Huchra, & Mould (1979). Thus, the Sakai et al. relation will give a slightly larger distance for NGC 5907, which has a larger velocity width than most galaxies in the sample, although the difference is well within the 0.36 magnitudes internal scatter.

For NGC 5907 itself, we adopt the values of $H_{-0.5} = 7.58$ and $\log W_{20}^c = 2.690$ given by Aaronson et al. (1982). For NGC 5907, the value of $\log W_{20}^c = 2.690$ is well-determined for this very edge-on system (e.g. Schöniger & Sofue 1994). The H magnitude of NGC 5907 may be more uncertain, as the galaxy is edge-on and internal extinction is likely to play a role even in the H-band. Two recent studies have attempted to determine the effect of extinction for spiral galaxies in the near-infrared. Based on a large study 154 spiral galaxies, Moriondo, Giovanelli, & Haynes (1998) find an extinction in H of approximately 0.15 magnitudes for a galaxy with the inclination

of NGC 5907. A smaller study by Tully et al. (1998) in K, finds 0.25 magnitudes of extinction in the K-band. We therefore adopt 0.2 magnitudes as the best estimate of the H-band extinction in NGC 5907, and note that the ~ 0.4 magnitudes scatter in the Tully-Fisher is sufficient to account for the uncertainties in this correction. With $\log W_{20}^c = 2.690$ and $H_{-0.5}^c = 7.38$, we find that the distance to NGC 5907 is 31.21, or 17.5 ± 2.7 Mpc, based on the Key Project relation.

An alternative is to use the slope found for spirals in Ursa Major and Virgo while still setting the zero point to give the same 16 Mpc distance to the Virgo cluster determined by HST Cepheid observations (Macri et al. 1999). Peletier & Willner studied roughly 25 spirals in each of these clusters and found a slope of $H_{-0.5}^c = -10.2(\log W_{20}^c - 2.5)$. We adopt the same zero point as above for the Key project sample, effectively setting the two Tully-Fisher relations equal for galaxies with $\log W_{20}^c = 2.5$. This approach gives a distance to NGC 5907 of 16.5 Mpc. The difference is due to the somewhat shallower slope found for the cluster surveys

A third approach is to take advantage of more modern two-dimensional H-band photometry of NGC 5907 (Barnaby & Thronson 1992). Although most calibration work is done with the Aaronson et al. (1982) aperture data, PW91 define a Tully-Fisher relationship based on the H-band light within the isophote at which the H-band surface brightness is brighter than 19 magnitudes/arcsec² (H_{19}). They find a Tully-Fisher relation for this isophotal magnitude of $\log (V_{20}) = -0.098(H_{19} - 9) + 2.525$, with the zero point set by $d_{Virgo} = 16$ Mpc. From two-dimensional photometry, Barnaby & Thronson (1992) derive face-on surface brightnesses and scale lengths for NGC 5907. Since the H_{19} magnitude of PW91 is defined within an isophote on the sky, it is dependent on galaxy inclination, with more light being encompassed for edge-on systems. We therefore translate the Barnaby & Thronson model to $i = 60$ deg, which is the most likely inclination in a random sample of galaxies. In this case, the H_{19} magnitude gives a distance of 12.9 Mpc based on the calibration above. Lower and upper limits to the distance derived from this technique can be derived by translating to edge-on and face-on system, giving a range in distances from 11.2 Mpc to 16.1 Mpc.

3.3.2. R-band Tully-Fisher

A somewhat independent check on the distance derived above can be obtained by considering the R-band rather than the H-band in the Tully-Fisher method. Morrison et al. (1994) estimated the reddening-free total magnitude of NGC 5907 of $m_R = 9.1$ by modelling the disk outside of the dust lane, and then extrapolating this model into the masked regions. Taking the R-band Tully-Fisher calibration of Pierce & Tully (1992, see also Jacoby 1992) and the rotation velocity given above, gives a distance of 14.3 Mpc. This R-band distance estimate is consistent with the H-band distance given above within the uncertainties of about 0.36 magnitudes for each technique.

3.3.3. Peculiar Velocity and Observed Density Field

The scatter in Tully-Fisher is not negligible, so it is important to consider other constraints on the distance to NGC 5907. One approach is to use the observed redshift of NGC 5907, and the expected peculiar velocity for a galaxy at its location to estimate its true distance. This requires a model for the underlying density field, which has been estimated both from IRAS galaxy surveys (Davis, Nusser, & Willick 1996) and optical galaxy surveys (Baker et al. 1998), using the expansion technique of Nusser & Davis (1994). The predicted peculiar velocity for NGC 5907 is then -250 km s^{-1} from the optical survey and -190 km s^{-1} for the IRAS survey. For field galaxies like NGC 5907, the uncertainty in these peculiar velocities is dominated by the random dispersion of galaxies around the smooth Hubble Flow, which is measured to be 120 km s^{-1} (e.g. Baker et al. 1999). Combined with $cz = 667 \text{ km s}^{-1}$ for NGC 5907 (RC3, de Vaucouleurs et al. 1991) and $H_0 = 70 \text{ km s}^{-1} \text{ Mpc}^{-1}$ for consistency with the Virgo distance above, we find distances of 13.1 and 12.2 Mpc respectively, with an uncertainty of $\pm 1.7 \text{ Mpc}$ due to random motions of galaxies. We account for the additional systematic uncertainty introduced by the Hubble Constant below.

3.3.4. Final Distance Estimate

To determine the distance to NGC 5907, we combine the Tully-Fisher and flow-field estimates in quadrature. For Tully-Fisher, we simply average the $H_{-0.5}^c$, H_{19} , and R-band estimates, for which we find 14.9 Mpc. Since the errors in these estimates are highly correlated, we retain an internal error of 0.36 magnitudes, or $\pm 2.3 \text{ Mpc}$. Similarly, for the flow-field estimate, we simply average the results from the IRAS and optical galaxy predictions, which gives a distance of $12.7 \pm 1.7 \text{ Mpc}$. We then combine these in quadrature, obtaining an answer of $13.5 \pm 1.4 \text{ Mpc}$. Both techniques depend directly on the Hubble constant, for which we have adopted a value of $70 \text{ km s}^{-1} \text{ Mpc}^{-1}$ (e.g. Mould et al. 1999). We take the uncertainty in this value to be 12% accommodating the latest results on the calibration of the Cepheid Period-Luminosity relationship (e.g. Maoz et al. 1999). Combining this uncertainty in the overall calibration of the distance scale with the uncertainties intrinsic to the techniques applied to NGC 5907, we find that the distance to NGC 5907 is $13.5 \pm 2.1 \text{ Mpc}$. For most of the work in this paper, we round this up to 14 Mpc.

The model luminosity functions in Figures 4 and 5 are based on this distance. In order for the detection of at most one star in our NICMOS image to be consistent with a Salpeter IMF and within 2σ of published optical colors, NGC 5907 would have to be at a distance of more than 24 Mpc, which is 5σ larger than our estimated distance of $14 \pm 2 \text{ Mpc}$. We also note that the distance we derive is larger than previously published distances, so accounting for the absence of bright giants in the extended light around NGC 5907 would require even larger discrepancies with earlier work.

3.4. R-band Surface Brightness

The predicted star counts are normalized so that their integrated flux produces the observed R-band surface brightness; therefore uncertainties in the surface brightness propagate to uncertainties in the predicted NICMOS counts. The R-band surface brightness within our NICMOS pointing is 25.85 ± 0.15 mag/arcsec 2 based on a direct measurement from the reduced R-band image of Morrison et al. (1994), kindly provided by H. Morrison and J. Monkiewicz. Independent measurements of the surface brightness in narrower filters at roughly the same wavelengths give good agreement on the surface brightness of the diffuse stellar component out to $R < 27$ mag/arcsec 2 (Zhang et al. 1999). Thus, the uncertainty in the surface brightness within our NICMOS field is small compared to other uncertainties and to the dramatic difference between the number of giants expected and the number observed in the NICMOS image.

4. Conclusions

The fundamental result of our investigation is that we detect only one unresolved object in our NICMOS images of the stellar halo of NGC 5907, compared to more than 100 giant stars that are expected to be observable within this field, given the observed surface brightness and colors in the region of our pointing and the simplest assumptions about the stellar population of the halo and the distance to the galaxy. Taken at face value, this result indicates that the dwarf to giant ratio is about 100 times greater than that for typical stellar populations.

Given the dramatic nature of this result, we consider other options. A very low metallicity ($[\text{Fe}/\text{H}] \lesssim -1.7$) results in giants too faint to be seen by our observations. However, a stellar population with such a low metallicity and a Salpeter IMF has colors for the integrated light that are more than 3σ bluer than the $(B - V)$ and $(V - I)$ observations of Lequeux et al. (1998). Alternatively, if NGC 5907 is more distant than typically believed, then the giants may be too faint to be observed. However, for a stellar population with a Salpeter IMF and a metallicity that gives colors within 2σ of the observed optical colors, the distance must be more than 24 Mpc to be even marginally consistent with our detection of only one stellar object. This is 5σ greater than our estimate of 14 ± 2 Mpc for the distance to NGC 5907, and even more discrepant with earlier work, which adopted closer distances (e.g. Morrison et al. 1994, Yost et al. 1999). Thus, only the “last resort” option of a stellar population with a very high dwarf-to-giant ratio appears to be able to account for the absence of resolved stars in our NICMOS image in the stellar halo of NGC 5907 without conflict with other observational data. Specifically, for a simple power-law parametrization of the IMF, $\alpha > 3$ is required to be within 2σ of the published $(B - V)$ and $(V - I)$ colors and within the 99% confidence limit of the detection of at most one star.

If confirmed, this result has important implications for the nature of the diffuse light observed at z -heights of 4–8 kpc in NGC 5907. Firstly, our observations do not support a number of proposed origins for this stellar component. Specifically, if this diffuse light originated from an

accreted elliptical galaxy (Lequeux et al. 1998), was dynamically heated from a thinner stellar disk, or is a tidal warp or ring (Shang et al. 1998), many giants would have been observed in our NICMOS images of NGC 5907, since none of these populations is expected to have an extremely steep IMF or a very low metallicity. Although a larger distance to NGC 5907 would allow any model of the extended stellar light in NGC 5907 to be reconciled with the data, no extant model provides an *a priori* explanation why several different techniques should underestimate the distance to NGC 5907. Very speculatively, if a high dwarf-to-giant ratio is the source of the absence of giants in our NICMOS images, and the IMF is assumed to be a power-law extended to masses less than $0.1 M_{\odot}$, then the R-band mass-to-light ratio is high enough that the observed halo can constitute the mass that produces the galaxy’s rotation curve. However, such a model is inconsistent with the combination of a non-detection of the halo of NGC 5907 at $3.5 - 5\mu$ and current models of stellar atmospheres of stars at the hydrogen burning limit (Yost et al. 1999).

Because a dramatically dwarf-rich stellar population has not been observed elsewhere, we consider several additional ways to constrain the nature of the observed stellar halo of NGC 5907. Although a stellar population with low metallicity and a standard IMF is not consistent with the published optical and near-infrared colors, measurements of colors at faint surface brightnesses are difficult. An independent, direct test of the low metallicity hypothesis can be made through WFPC2 observations. These should see thousands of giants if the observed halo light in NGC 5907 comes from metal-poor stars with a standard IMF and the distance of the galaxy is consistent with existing estimates. However, if the WFPC2 observations yield a null result, it will be difficult to obtain further independent tests of the distance to NGC 5907. One possibility is to obtain NICMOS observations closer to the center of the galaxy, which should reveal some bright stars if the distance to the galaxy is not much greater than expected. Initial HST observations of its globular cluster system did not reveal a sufficient number of clusters to reliably use the peak of the globular cluster luminosity function as a distance indicator (Kissler-Patig et al. 1999). Planetary nebulae might be observable, although observations in the halo could be suspect if the IMF is as dramatically different as suggested here.

We thank Stéphane Charlot for providing us with the isochrone synthesis data for galaxy evolution. We thank Heather Morrison and Joe Silk for valuable discussions, and the referee for helpful suggestions. We also thank Heather Morrison and Jackie Monkiewicz for providing direct measurements of the optical surface brightness in their images within our NICMOS field. We acknowledge excellent assistance from Doug van Orsow at STScI in getting our program executed and financial support from the following HST NASA grants GO-07277 (SEZ and FRM) and AR-07523 (FRM). FRM also acknowledges an IoA postdoctoral research fellowship.

REFERENCES

Aaronson, M., et al. 1982, ApJS, 50, 241

Aaronson, M., Huchra, J., & Mould, J. 1979, 229, 1

Ashman, K. M. 1992, PASP, 104, 1109

Bahcall, N.A., Lubin, L.M. & Dorman, V. 1995, ApJ, 477, L81

Baker, J.E., Davis, M., Strauss, M.A., Lahav, O., & Santiago, B.X., 1998, ApJ, 508, 6

Barnaby, D. & Thronson, H.A., 1994, AJ, 107, 1717

Bruzual, G. & Charlot, S. 1998, private communication

Burles, S., & Tytler, D. 1998a, ApJ, 499, 699

Burles, S., & Tytler, D. 1998b, ApJ, 507, 732

Cohen, M. 1993, AJ, 105, 1860

Colina, L., & Rieke, M.J. 1997, in The 1997 HST Calibration Workshop, eds. et al. (STScI: Baltimore), 182

de Vaucouleurs, G., de Vaucouleurs, A., Corwin, H.G., Buta, R., Paturel, G., & Fouque, P. 1991, Third Reference Catalog of Galaxies (RC3)

Davis, M. 1975, AJ, 80, 188

Davis, M., Nusser, A., & Willick, J.A. 1996, ApJ, 473, 22

Efstathiou, G., Ellis, R. S., & Peterson, B. A. 1988, MNRAS, 232, 431

Fuchs, B. 1995, A&A, 303, L13

Harris, W.E., & Racine, R. 1979, ARAA, 17, 241

Jacoby, G., et al. 1992, PASP, 104, 599

James, P., & Casali, M. M. 1998, MNRAS, 301, 280

King, I.R., et al. 1998, ApJ, 492, L37

Kissler-Patig, M., Ashman, K.M., Zepf, S.E., & Freeman, K.C. 1999, AJ, 118, 197

Krist, J. 1993, in Astronomical Data Analysis Software and Systems II, eds. R.J. Hanisch, R.J.V. Brissenden, & J. Barnes, ASP Conference Series 52, 536

Lejeune, Th., Cuisinier, F., Buser, R. 1997, A&AS, 125, 229

Lequeux, J., Fort, B., Dantel-Fort, M., Cuillandre, J.-C., & Mellier, Y. 1996, AA, 312, L1

Lequeux, J., Combes, F., Dantel-Fort, M., Cuillandre, J. -C., Fort, B., & Mellier, Y. 1998, AA, 334, L9

Liu, M.C., Marleau, F.R., Graham, J.R., Charlot, S., Sackett, P.D., & Zepf, S.E. 1998, Abstracts of the 19th Texas Symposium, eds. J. Paul, T. Montmerle, and E. Aubourg (CEA Saclay), 28

Loveday, J., Peterson, B.A., Efstathiou, G., & Maddox, S.J. 1992 ApJ, 390, 338

MacKenty, J., et al. 1997, NICMOS Instrument Handbook (Baltimore: STScI)

Macri, L., et al. 1999, ApJ, in press

Maoz, E., et al. 1999, Nature, 401, 351

Marleau, F.R., Graham, J.R., Charlot, S., & Liu, M.C. 1999, in preparation

McWilliam, A., Rich, R.M. 1994, ApJS, 91, 749

Moriondo, G., Giovanelli, R. & Haynes, M.P. 1999, A&A, 338, 795

Morrison, H. L., Borošon, T. A., & Harding, P. 1994, AJ, 108, 119

Morrison, H.L. 1999, in The Galactic Halo, ASP Conference Series , eds. B.K. Gibson, T.S. Axelrod and M.E. Putman, 174

Mould, J., et al. 1999, ApJ, in press

Mushotzky, R. F., Loewenstein, M., Awaki, H., Makashima, K., Matsushita, K., & Matsumoto, H. 1994, ApJ, 436, L79

Peletier, R.F., & Willner, S.P. 1993, ApJ, 418, 626

Peletier, R.F., & Willner, S.P. 1991, ApJ, 382, 382

Pierce, M.J. & Tully, R.B. 1992, ApJ, 387, 47

Racine R. 1991, AJ, 101, 865

Reitzel, D.B., Guhathakurta, P., & Gould, A. 1998, AJ, 116, 707

Rudy, R. J., Woodward, C. E., Hodge, T., Fairfield, S. W., & Harker, D. E. 1997, Nature, 387, 159

Sackett, P.D., Morrison, H.L., Harding, P., & Borošon, T.A. 1994, Nature, 370, 441

Sackett, P. D. 1996, IAU 173, Astrophysical Applications of Gravitational Lensing, eds. C. Kochanek and J. Hewitt, (Dordrecht: Kluwer), 165

Sackett, P.D. 1999, in Galactic Dynamics, ASP Conference Series, eds. D. Merritt, J.A. Sellwood and M. Valluri, in press (astro-ph/9903420)

Saha, A. 1985, ApJ, 289, 310

Salaris, M., & Cassisi, S. 1998 astro-ph/9803103

Sancisi, R. & van Albada, T.S. 1987, in IAU Symposium 117, eds. J. Kormendy and G.R. Knapp (Reidel:Dordrecht), 67

Shang, Z. et al. 1998, ApJ, 504, L23

Skrutskie, M. F., Shure, M. A., & Beckwith, S. 1985, ApJ, 299, 303

Sofue, 1994, PASJ, 46, 173

Stetson, P. B. 1992, ASP Conf. Ser. 25: Astronomical Data Analysis Software and Systems I, 1, 297

Tiede, G.P., Frogel, J.A., & Terndrup, D.M. 1995, AJ, 110, 2788

Trimble, V. 1987, AARA, 25, 42

Tully, R.B., Pierce, M.J., Huang, J-S., Saunders, W., Verheijen, M.A.W., & Witchalls, P.L. 1998, 115, 2264

Yan, L., McCarthy, P.J., Storrie-Lombardi, L.J., & Weymann, R.J. 1998, ApJ, 503, L19

Yost, S.A., et al. 1999, preprint (astro-ph/9908364)

Zaritsky, D. 1999, in The Galactic Halo, ASP Conference Series, eds. B.K. Gibson, T.S. Axelrod and M.E. Putman, 34

Zaritzky, D., Smith, R., Frenk, C., & White, S. D. M. 1993, ApJ, 405, 464

Zheng, Z. et al, 1999, AJ, 117, 2757

Zinn, R. 1985, ApJ, 293, 424

NGC 5907: R-band

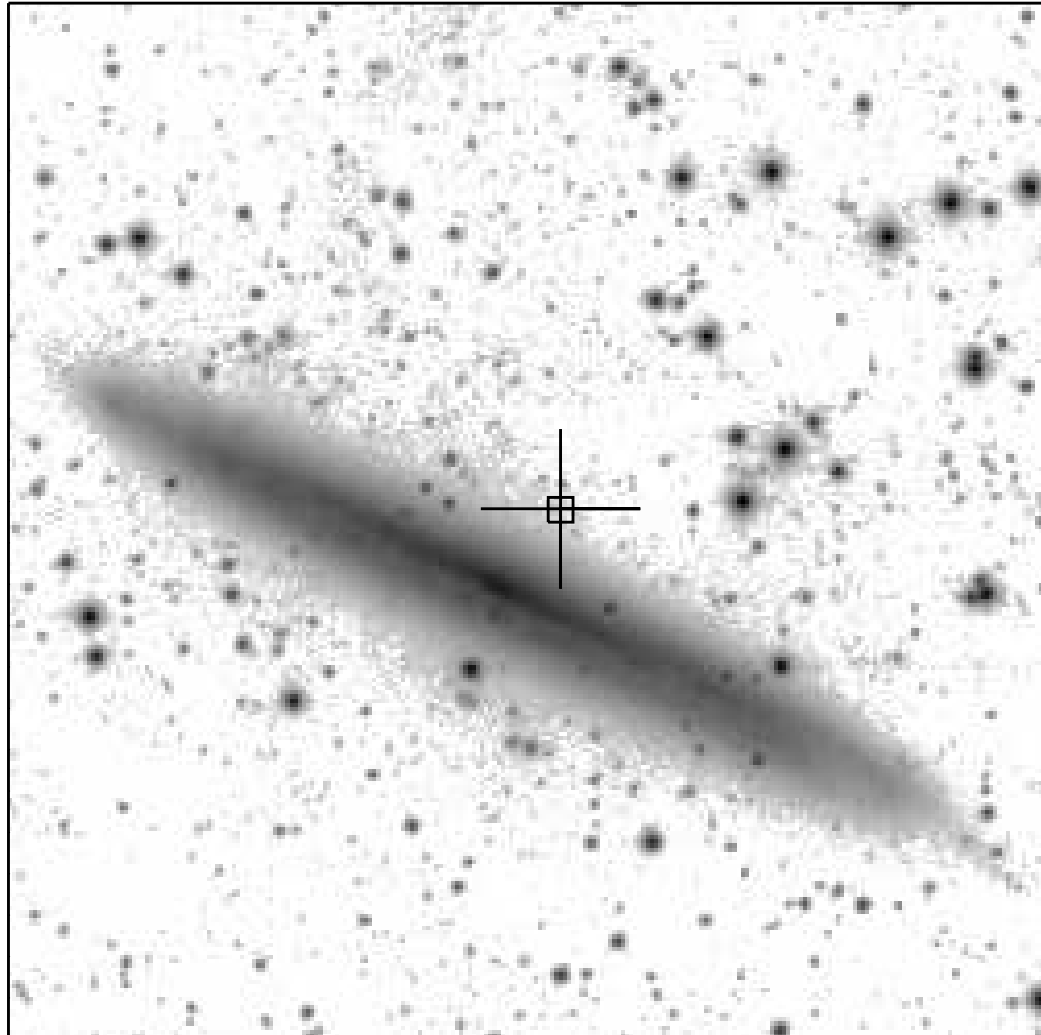


Fig. 1.— A deep R-band image of NGC 5907 from Morrison et al. (1994), with our NICMOS field overplotted as a square. The image is $12'.8$ on a side, and the NICMOS pointing is $75''$ above the plane of the disk. North is up and east is to the left.

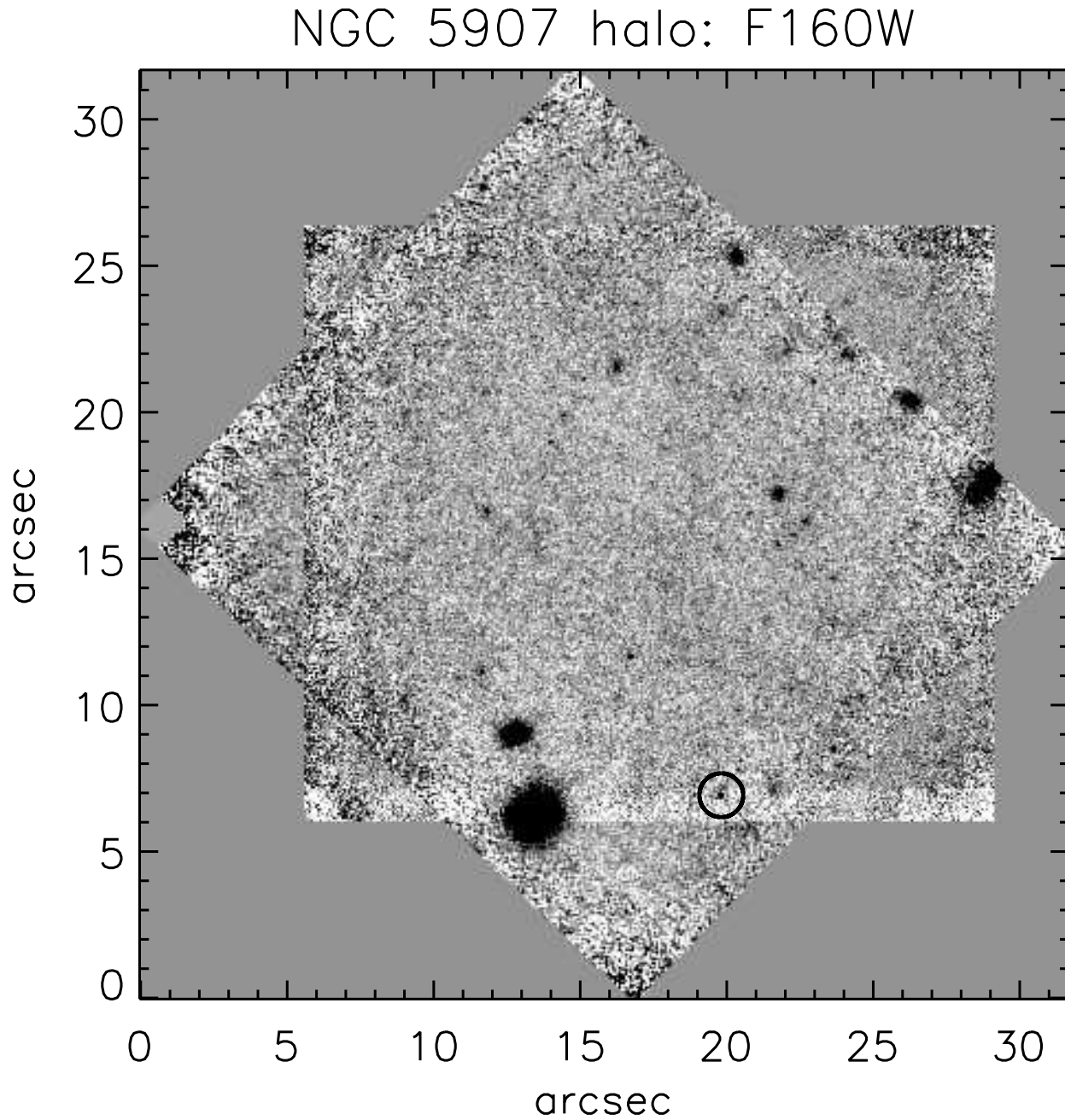


Fig. 2.— The NICMOS/F160W mosaic of our field in the halo of NGC 5907. The data show a single unresolved object (circled on the image) with $m_{\text{F160W}} = 23.6$ mag. The handful of other objects seen in the image are extended and thus identified as background galaxies.

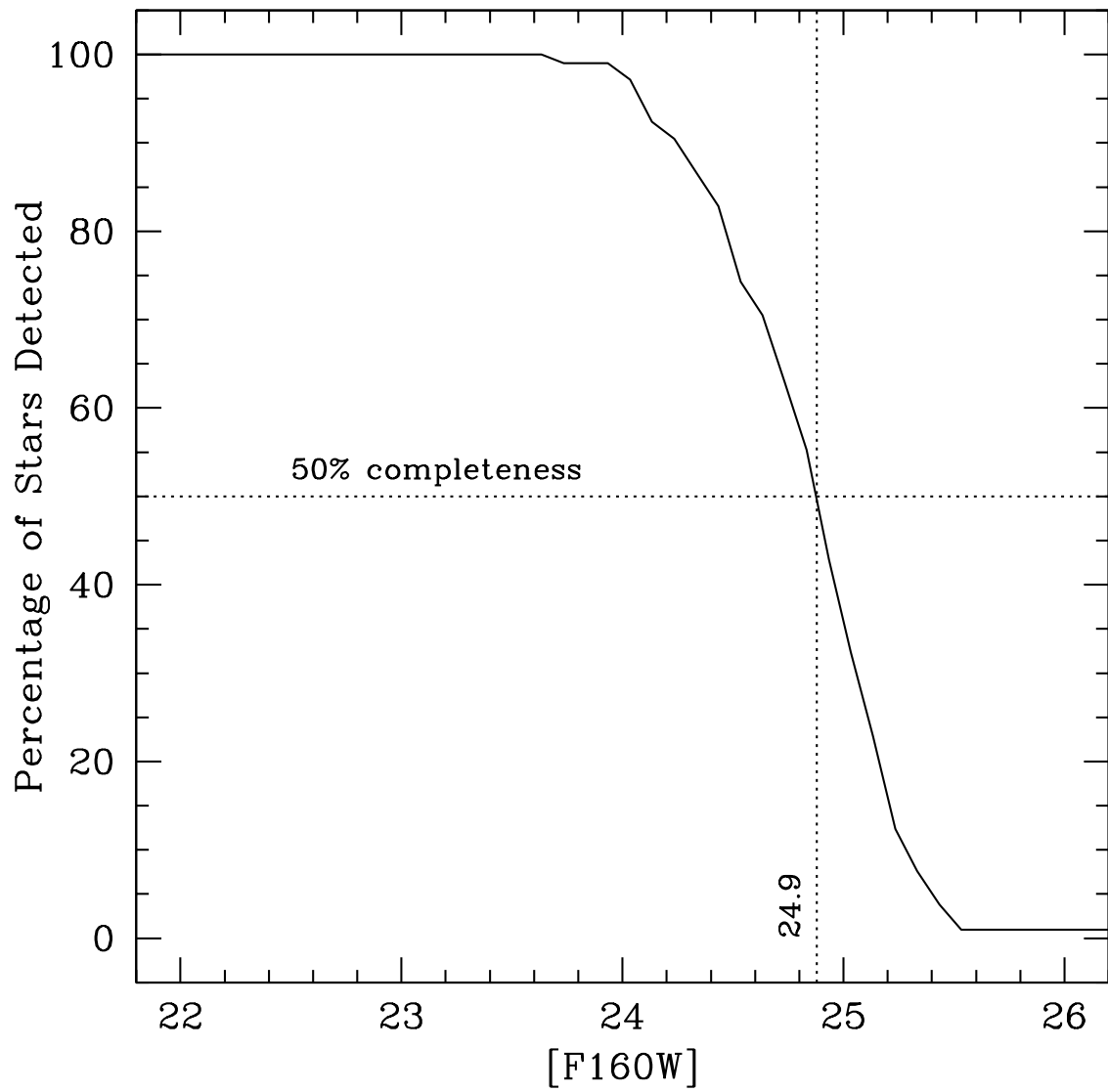


Fig. 3.— A plot showing the completeness of our photometry as a function of magnitude.

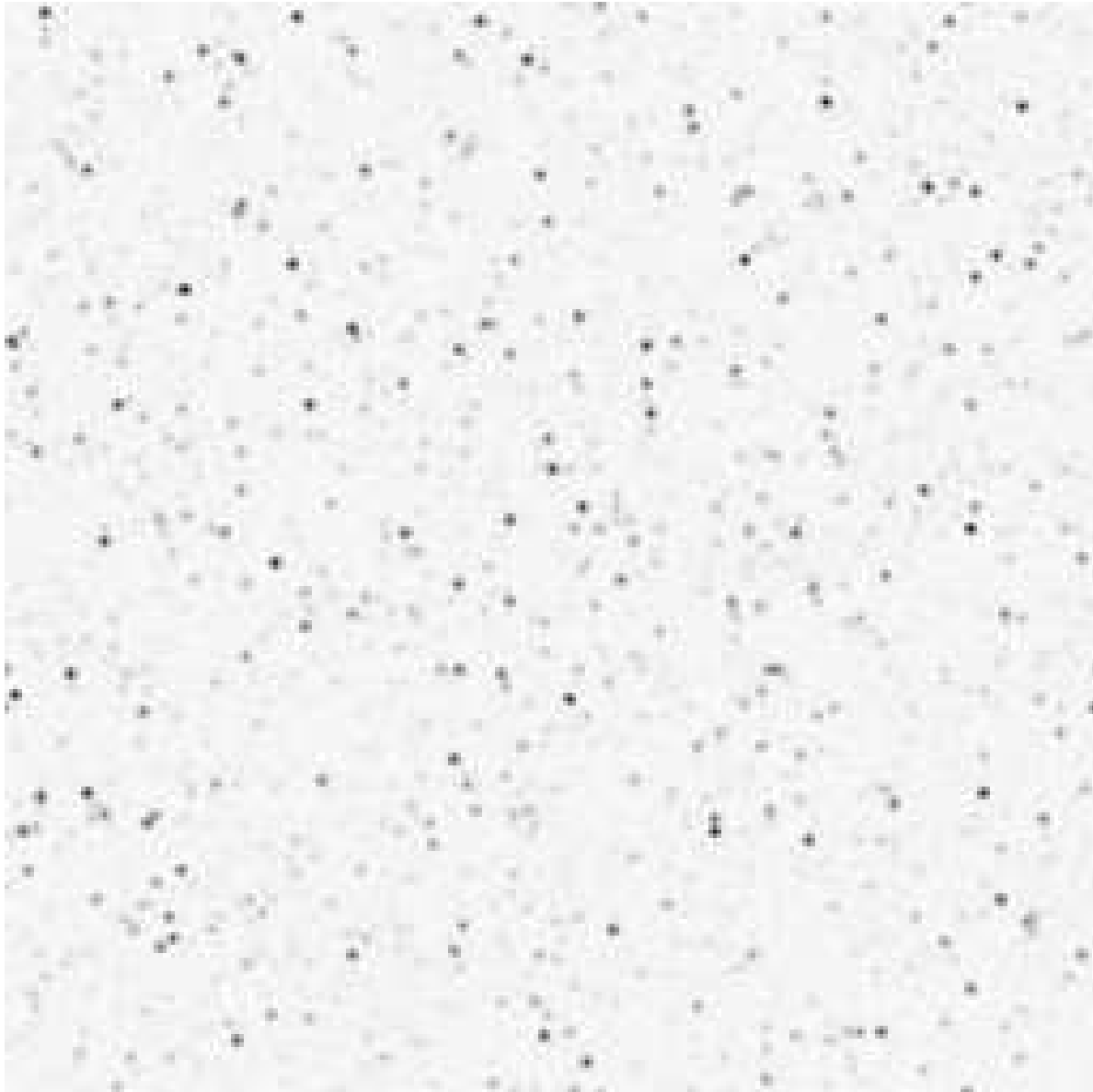


Fig. 4.— A simulation of the expected appearance of our NICMOS images of the NGC 5907 halo assuming a stellar population like that of the Galactic bulge, as suggested by the red optical and near-infrared colors of the integrated light, and normalized to the observed integrated surface brightness of Morrison et al. (1994). This simulated image is $19''2$ on a side.

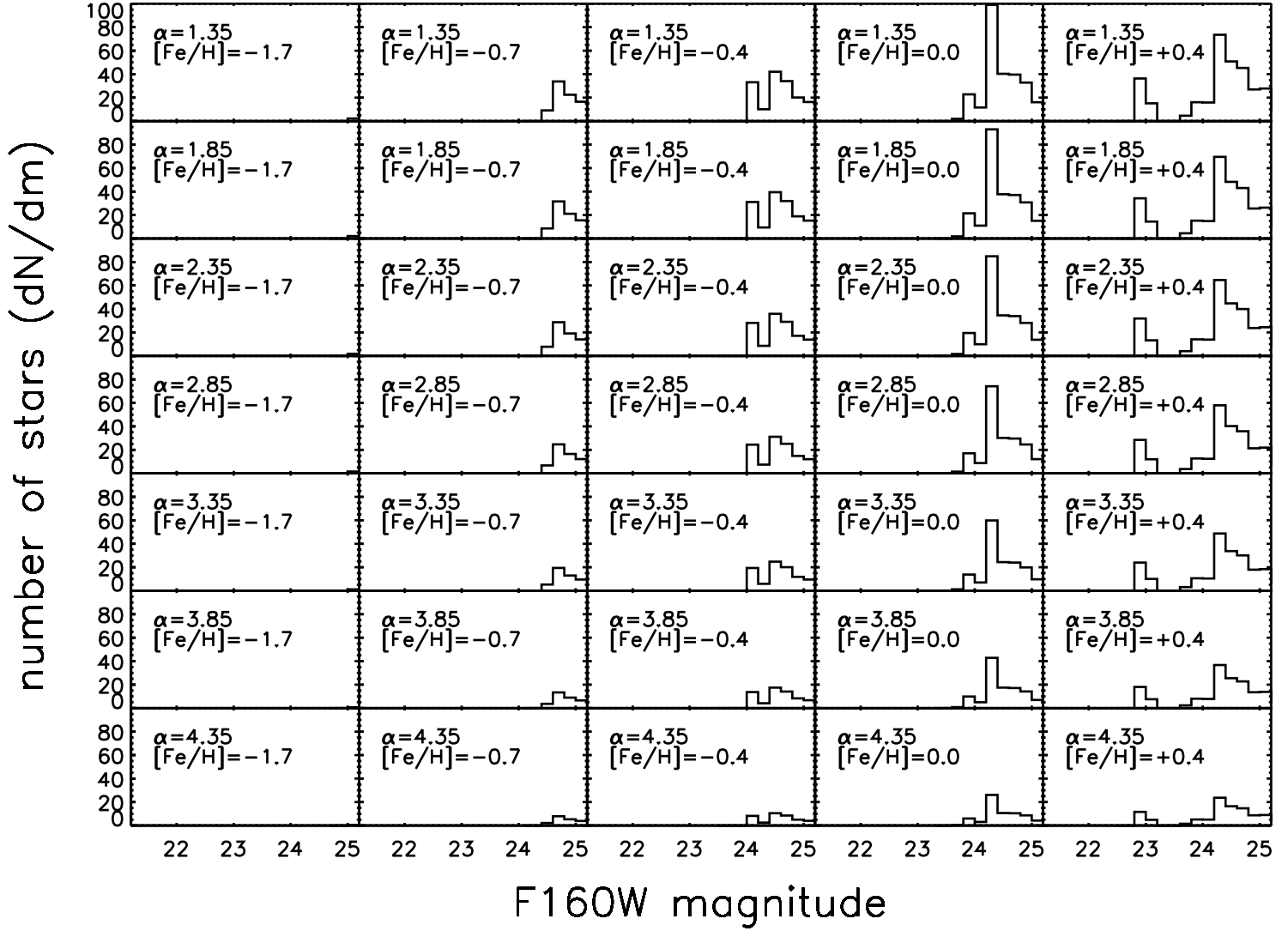


Fig. 5.— The predicted luminosity functions for our NICMOS observations. The predicted number of stars as a function of magnitude is based on a stellar population model with the given initial mass function and metallicity, convolved with the completeness function given in Figure 3. Most models predict several tens to hundreds of stars should be observed in our NICMOS field, but we observe only one potential star, with a magnitude of $m_{F160W} = 23.6$. This observation allows only models of the stellar population within our NICMOS field in the halo of NGC 5907 with either very low metallicity ($[\text{Fe}/\text{H}] \lesssim -1.7$) or a very steep IMF ($\alpha > 4.35$).

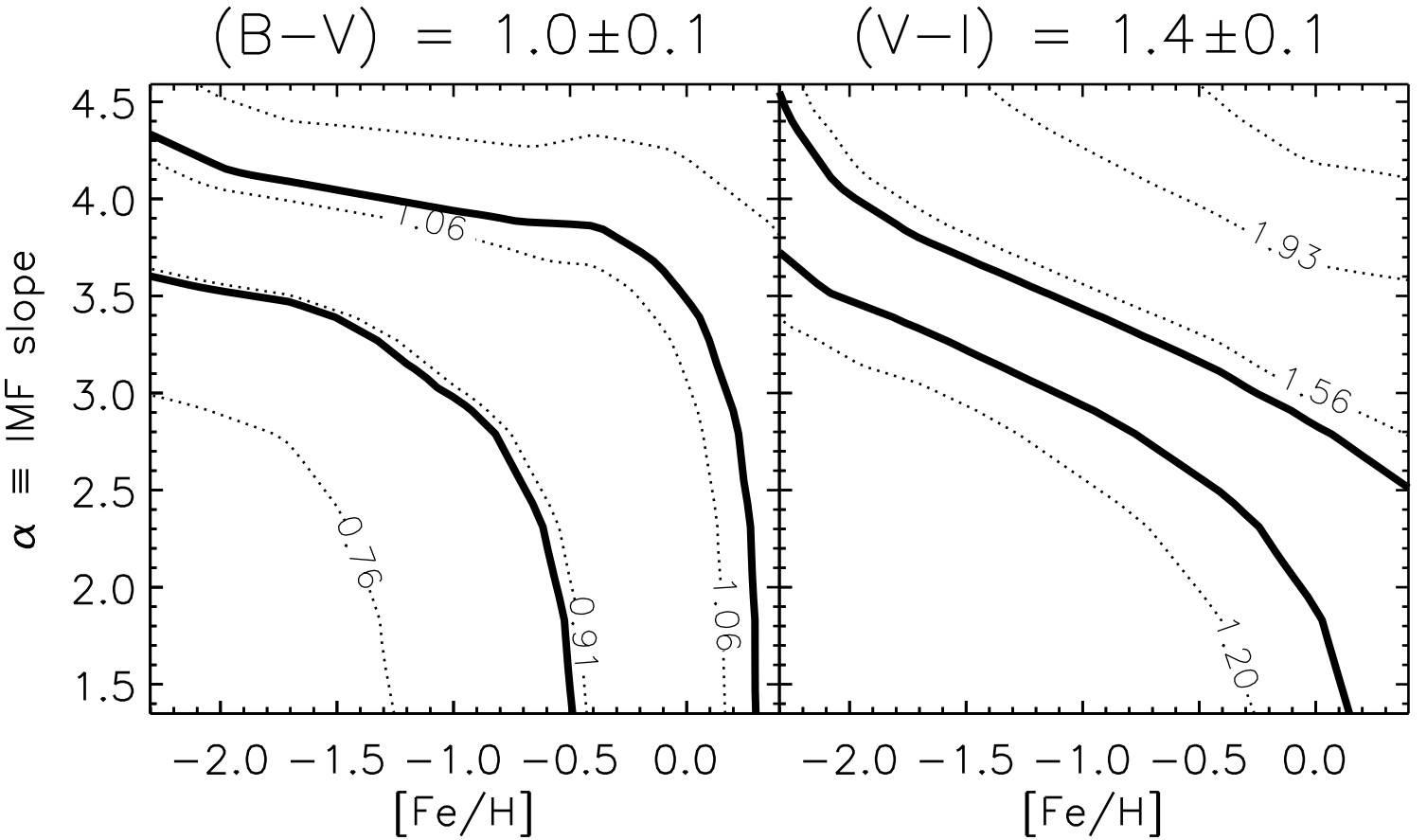


Fig. 6.— Constraints on the stellar population from the observed integrated colors of the halo of NGC 5907. The colors and the errors are from Lequeux et al. (1998). The range of IMF slope α and $[\text{Fe}/\text{H}]$ are the same as those used in Figure 5. The light contours show the trends in this diagram for fixed color. The solid line represents the 1σ limit of the published colors. This plot shows that the published colors are strongly inconsistent with a low $[\text{Fe}/\text{H}]$, normal α stellar population that might otherwise account for the absence of giants in the NICMOS images.